8 Biological Science

8-1 Crystal Structure of Thymine DNA Glycosylase Conjugated to SUMO-1 or SUMO-3

SUMO is a ubiquitin-like modifier protein, and can be covalently bound to the lysine residue of a target protein through an enzymatic pathway homologous with that used in ubiquitination (ubiquitin conjugation) [1]. SUMOylation regulates a vast variety of cellular events such as chromatin structure formation, transcription, DNA repair, chromosome segregation and ion channel activity, and does not rely on degradative signaling through the proteasome or lysosome [2]. SUMOylation is generally thought to modulate the protein-protein or protein-DNA interactions of the target proteins, thereby raising their functional transfers. Whether SUMOylation can induce a structural rearrangement of target proteins has been a matter of speculation.

While yeast *Saccharomyces cerevisiae* has only one SUMO isoform (Smt3), four isoforms (SUMO-1 to SUMO-4) have been found in mammals. SUMO-2 and SUMO-3 have highly homologous sequences, and constitute a subgroup distinct from SUMO-1 [3]. The functional differences between modifications by SUMO-1 and SUMO-2/3 have not yet been well elucidated.

Thymine DNA glycosylase (TDG), a SUMO substrate protein, is an enzyme that is indicated to be involved in the base excision repair (BER) of G-U or G-T mismatched DNA. TDG is thought to initiate the BER pathway by releasing uracil or thymine from the mismatched DNA [1,4] . Following the base excision, TDG tightly binds in vitro to its product, the abasic site. Upon SUMOylation, TDG loses its binding affinity to the abasic site, suggesting that SUMOylation promotes the release of TDG from the DNA site [1].

In order to reveal the molecular mechanism of the SUMOylation-dependent loss of the DNA binding activity of TDG, we have determined the crystal structure of the central region of TDG (residues 112-339) conjugated to SUMO-1 at 2.1-Å resolution. The central region consists of the catalytic core domain (residues 117-300), the C-terminal segment (residues 301-330) containing the SUMOylation site, Lys330, and the flanking regions of TDG. Figure 1 shows a ribbon diagram of the crystal structure. The catalytic core domain, the C-terminal segment and SUMO-1 are shown in blue, orange and green, respectively. The C-terminal segment forms a major interface of TDG with SUMO-1. In addition to the covalent binding that occurs at the SUMOylation site, Lys330, the segment makes non-covalent contacts with SUMO-1 by forming an antiparallel β-sheet with a β-strand of SUMO-1. The region of the C-terminal seg-
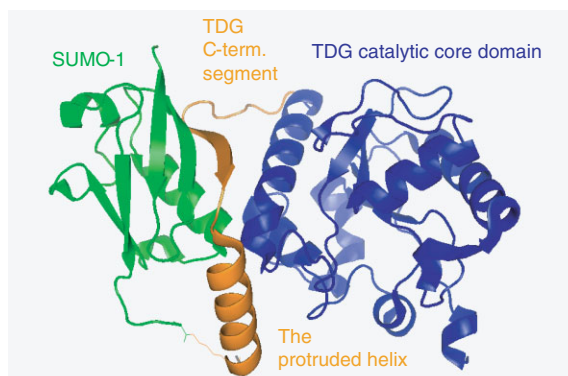

Figure 1
Ribbon diagram of the crystal structure of the central region of TDG conjugated to SUMO-1. The main and side chains of the isopeptide bond-forming residues, Lys330 of TDG and Gly97 of SUMO-1, are also shown in wire-frame.
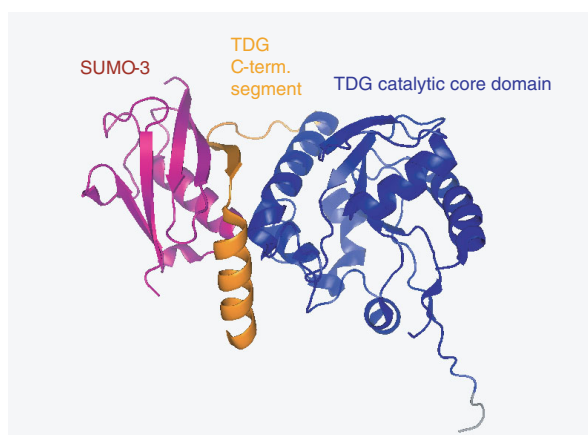

Figure 2
Ribbon diagram of the crystal structure of the central region of TDG conjugated to SUMO-3.

ment of TDG, which is flanked by the covalent and non-covalent contact sites with SUMO-1, possesses a helix protruding from the protein surface.

We have built a model of the complex formed by the central region of TDG conjugated to SUMO-1 and a DNA containing the abasic site [5]. For the model building, the coordinates of the TDG core domain in the crystal structure of the central region of TDG conjugated to SUMO-1 were best-fitted to be superposed on those of *Esherichia coli* G:T/U mismatch-specific DNA glycosylase bound to a DNA containing the abasic site (PDB code 1MWI [6]). In the model, the helix protruding from the C-terminal segment of TDG is positioned so as to make a steric clash with the sugar-phosphate backbone of the DNA.

We have also determined the crystal structure of the central region of TDG conjugated to SUMO-3 at 2.1-Å resolution (Fig. 2). Although electron densities of the residues involved in the isopeptide bond formation are missing, the overall structure of the central region of TDG conjugated to SUMO-3 is similar to that of the SUMO-1-conjugated form.

M. Shirakawa[1,2,3] and D. Baba[1,4,] (**[1]Kyoto Univ., [2]RIK-EN-GSC, [3]CREST, Japan Sci. and Tec. Cor, [4]Yokohama City Univ.**)

References
[1] U. Hardeland, R. Steinacher, J. Jiricny and P. Schär, *EMBO J.,* **21** (2002) 1456.
[2] R. T. Hay, *Mol. Cell,* **18** (2005) 1.
[3] K. I. Kim, S. H. Baek and C. H. Chung, *J. Cell. Physiol.*, **191** (2002) 257.
[4] U. Hardeland, M. Bentele, T. Lettiere, R. Steinacher, J. Jiricny and P. Schär, *Prog. Nucleic Acid Res. Mol. Biol.*, **68** (2001) 235.
[5] D. Baba, N. Maita, J. G. Jee, Y. Uchimura, H. Saitoh, K. Sugasawa, F. Hanaoka, H. Tochio, H. Hiroaki and M. Shirakawa, *Nature*, **435** (2005) 979.
[6] T. E. Barrett, R. Savva, T. Barlow, T. Brown, J. Jiricny and L. H. Pearl, *Nature Structural Biology*, **5** (1998) 697.

8-2 Double-Sided Ubiquitin Interacting Motif of Hrs in Protein Sorting

Degradation control is an essential mechanism of protein regulation and quality control. Monoubiquitination plays an important role in the degradation of integral membrane proteins [1] whereas K48-linked ubiquitin chain fills a key role in soluble protein degradation.

Targeted membrane proteins are known to be (multi-) monoubiquitinated when they degrade. The monoubiquitinated proteins are sorted into multivesicular bodies, which then fuse with lysosomes. Hepatocyte-growth factor-regulated trypsine-kinase substrate (Hrs) is one of the essential proteins for this sorting mechanism [2]. Hrs interacts with ubiquitin by its ubiquitin interacting motif (UIM). The ability to bind ubiquitin is essential for the function of Hrs in sorting ubiquitinated proteins [3].

In order to understand the molecular mechanism of ubiquitin recognition by Hrs, we attempted to crystallize a ubiquitin/Hrs-UIM complex. Using the hanging-drop vapor-diffusion method, we obtained high-quality crystals allowing X-ray diffraction measurements to be performed. Datasets were collected using synchrotron radiation of 1.0-Å wavelength at beamline AR NW12A. We obtained 1.7-Å-resolution data with good statistics (R_{merge} = 5.1%). Using the molecular replacement method, we have determined the complex structure [4].

The complex consists of two ubiquitin molecules and one UIM peptide. The UIM forms a single α-helix which binds two ubiquitin molecules on either side of the helix (Figs. 3(a, b)). Both ubiquitin molecules interact with the UIM in the same manner. The interaction surfaces of both ubiquitin molecules consist of L8, R42, I44, G47, Q49, H68, V70 and R72, involving a common interaction surface of ubiquitin termed the "I44 surface". One ubiquitin interacts with E259, E262, L263, L265, A266, L267, L269, S270, Q271 and E273 of UIM. Another ubiquitin interacts with E261, Q264, L265, L267,

A268, L269, Q271, S272 and E273 (Figs. 3(c, d) and Fig. 4(a)). To find the double-binding sites, bindings with Hrs-UIM and its mutants were assayed. Compared with the wild type UIM, the single mutants A266Q and A268Q can bind to only half the amount of ubiquitin, and the double mutant A266Q A268Q cannot bind at all to ubiquitin (Fig. 4(b)). These results support the double binding sites of UIM in the crystal structure. We also found that the double-binding sites should be intact for efficient function of Hrs *in vivo* [3].
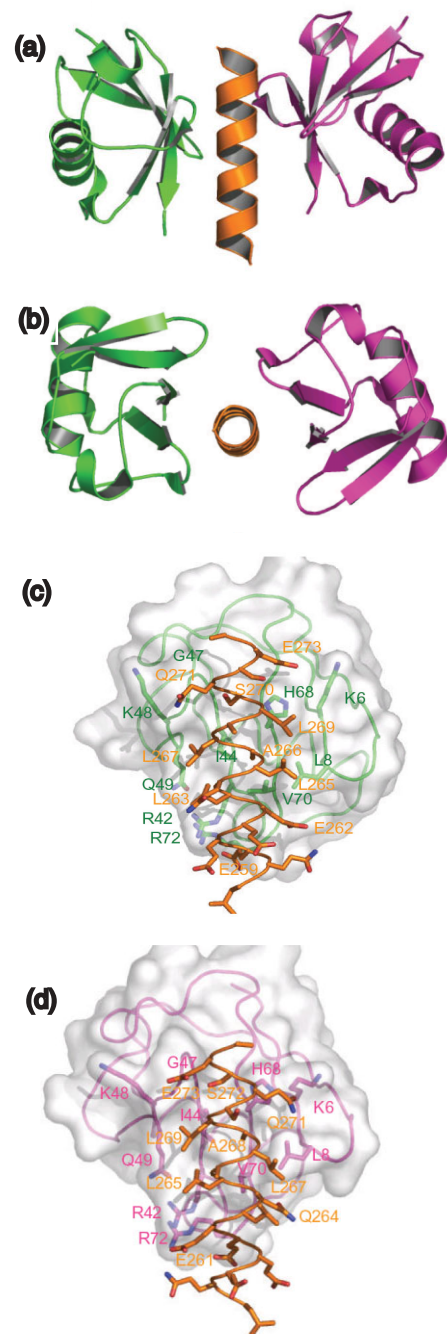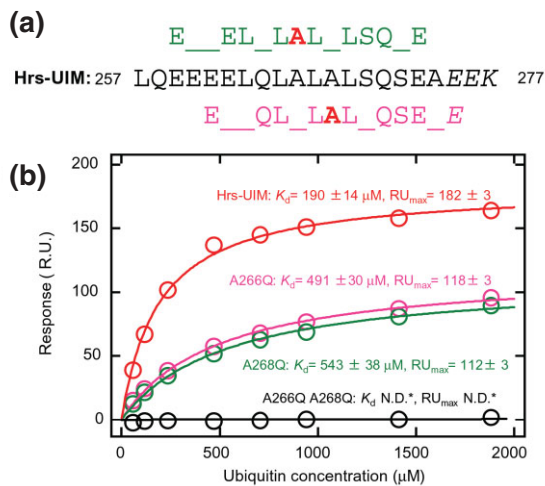
Figure 3

(a,b) Overall structure of the complex between Hrs-UIM and two ubiquitin molecules. *Green*, ubiquitin molecule A; *pink*, molecule B; *orange*, UIM. Shown are side view (a) and top view (b). (c,d) Sites of interactions between Hrs-UIM and ubiquitin molecules A (c) and B (d). Residues involved in binding of ubiquitin molecules to Hrs-UIM are indicated, and the coloring is as in (a) and (b). *Red* and *blue* indicate oxygen and nitrogen atoms, respectively.

(a)


```
          E__EL_LAL_LSQ_E
Hrs-UIM: 257 LQEEEELQLALALSQSEAEEK  277
          E__QL_LAL_QSE_E
```

(b)

Figure 4
(a) Repeating sequence of Hrs-UIM. The *middle* line shows the sequence of Hrs-UIM; the *top* and *bottom* lines show motifs binding ubiquitin molecule A (*green*) and molecule B (*pink*) with A266 and A288 in red. *Italic letters* indicate residues not observed in the electron density map. The two motifs are shifted by two residues relative to each other. (b) Surface plasmon resonance biosensor assay of the Hrs-UIM/ubiquitin interaction. For each experiment, GST-fused Hrs-UIM was immobilized on an anti-GST antibody-coated surface, over which ubiquitin was injected as analyte at the indicated concentrations. Circles and curves in *red, pink, green* and *black* indicate wild type Hrs-UIM, A266Q, A268Q and A266Q A268Q mutants, respectively. Estimated binding affinities and saturated values of the response change are given. N.D.: Not detected.

An important feature of Hrs-UIM for double-sided binding is the self-repeating sequence, i.e., the key residues of the first binding site are repeated at sites shifted by two residues along the UIM sequence (Fig. 4(a)). On the basis of our results, we propose a new double-sided UIM, e-x-e-x-φ-x-φ-A-φ-A-z-S-z-S/A-e where e denotes a negatively charged residue, φ a hydrophobic residue and z a bulky hydrophobic or polar residue. Indeed, a sequence search yielded a number of putative double-sided UIMs. Furthermore, we found that some of the candidates are actually double-sided UIMs.

The double binding sites may show remarkably higher affinities to multi-monoubiquitinated proteins than a single binding site, since two ubiquitin molecules which link the same protein can bind to a double-sided UIM at the same time. This double-sided binding of Hrs-UIM would be an essential feature in the efficient binding of multi-monoubiquitinated protein complexes.

S. Hirano[1], M. Kawasaki[1], H. Ura[1], R. Kato[1], C. Raiborg[2], H. Stenmark[2] and S. Wakatsuki[1] ([1]KEK-PF, [2]Univ. of Oslo)

References
[1] C. Raiborg and H. Stenmark, *Cell Struct. Funct.,* **27** (2002) 403.
[2] C. Raiborg, T. E. Rusten and H. Stenmark, *Curr Opin Cell Biol.,* **15** (2003) 446.
[3] C. Raiborg, K. G. Bache, D. J. Gilloly, I. H. Madshus, E. Stang and H. Stenmark, *Nature Cell Biol.,* **4** (2002) 394.
[4] S. Hirano, M. Kawasaki, H. Ura, R. Kato, C. Raiborg, H. Stenmark and S. Wakatsuki, *Nat Struct. Mol. Biol.*, **13** (2006) 272.

8-3 Structural Basis of a Toxin-Antitoxin Complex: YefM-Induced Rearrangement of the YoeB Catalytic Site

Eubacteria that cause nosocominal infections retain plasmid DNA that has acquired antibiotic-resistant genes. Such DNA is stably maintained in the bacteria by two types of proteins, toxin and antitoxin, which are known as addiction modules. These modules were originally identified as stabilization factors for plasmids of low copy number. Daughter cells lacking the plasmid are killed by the stable toxin once the unstable antitoxin has been degraded by host proteases, whereas those inheriting the plasmid survive (Fig. 5). Bacterial chromosome also encodes some pairs of genes of these proteins in free-living prokaryotes. It has been proposed that the modules function as bacterial programmed cell death, but recent studies indicates that these proteins modulate global levels of translation through RNA degradation by toxin and the inhibition by the antitoxin during nutritional and/or environmental stress. Of these *Escherichia coli* chromosomal toxins, MazF is characterized as an ACA sequence specific endoribonuclease (RNase) and RelE is characterized as a codon-dependent RNase that is active only when it is associated with the ribosomal A-site.

The YefM-YoeB antitoxin-toxin module on the *E. coli* chromosome was originally identified by homology with the Axe (antitoxin)-Txe (toxin) pair of the *Enterococcus faecium* pRUM multidrug-resistant plasmid. Like other plasmid addiction modules, the YoeB toxin is a basic protein, whereas the YefM antitoxin is acidic and structurally unfolded. The yefM-yoeB gene cassette functions as an antitoxin-toxin module. YoeB toxin induces cleavage of translated mRNA. To understand the relationship between the RNase activity of the YoeB toxin and inhibition by the YefM antitoxin, we have determined the crystal structures of the *E. coli* YefM-YoeB complex and two crystal forms of the YefM-free YoeB toxin, using diffraction data collected at BL41XU of SPring-8 and at BL-5A, respectively.

In contrast to the structure of the *E. coli* MazEF antitoxin-toxin complex [1], the structure of the YefM-YoeB complex has a 2:1 heterotrimeric form (Fig. 6A) [2]. One of the C-terminal peptide regions of the YefM homodimer exclusively interacts with an atypical microbial RNase fold of YoeB while the other projects into the solvent to be disordered. This asymmetric organization of the C-terminal regions of the YefM dimer relative to the YoeB monomer is essential for the 2:1 complex formation. Biochemical analyses and mutagenesis experiments have identified that YoeB preferentially cleaves at the 3' end of purine ribonucleotides and that three residues (Glu46, Arg65 and His83) of YoeB are responsible for the RNase activity. Comparison with the YefM-free YoeB structure reveals a conformational rear-
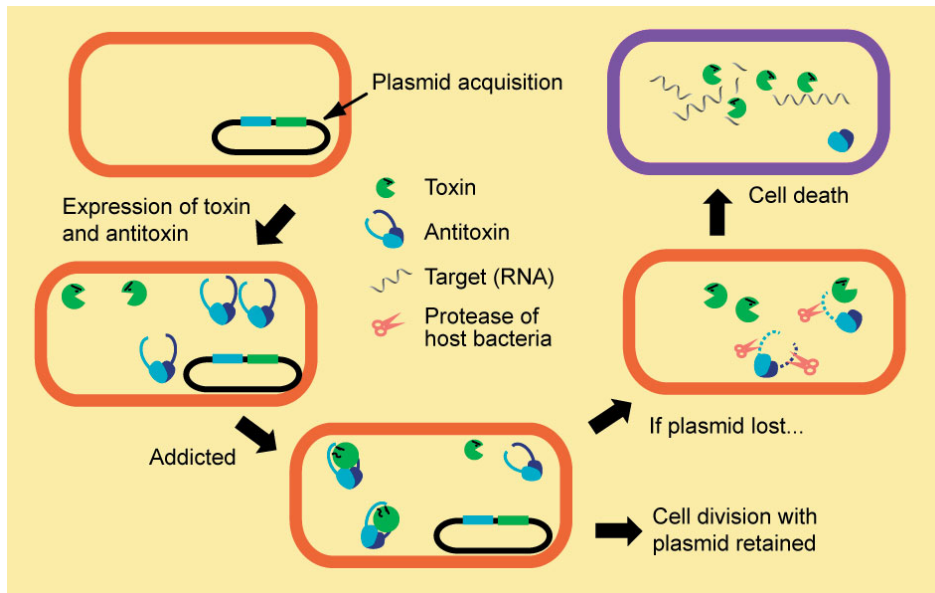
Figure 5

Model for Plasmid Addiction TA System. In the plasmid-containing cell, both antitoxins and toxins are present. The cells in which toxin is inactivated by antitoxin are viable. If plasmid is not inherited during cell division, a plasmid-cured daughter cell is produced and the antitoxin is no longer synthesized. As the unstable antitoxin is degraded by host protease, the stable toxin can interact with its target, thus causing cell death.
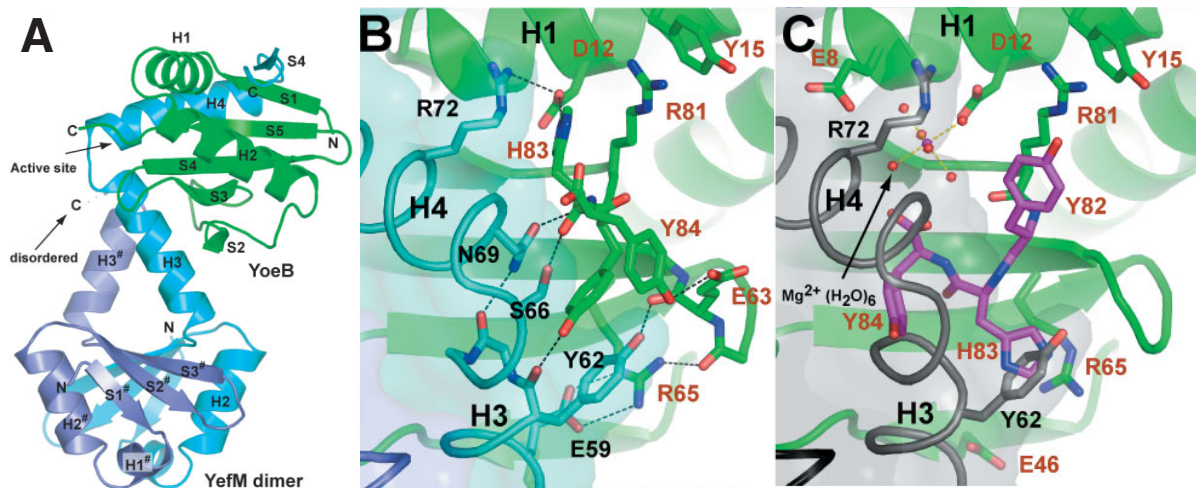

Figure 6

(A) Ribbon drawing of the asymmetric YefM homodimer with ordered (cyan) and disordered (lavender) C-termini bound to the YoeB monomer (green), viewed along an axis perpendicular to the 2-fold axis of the YefM N-terminal dimeric structure. (B) The active site conformation of YoeB bound to YefM. (C) YefM-free conformation of YoeB. The three C-terminal amino acids of YoeB (magenta carbon) change to the active conformation for RNA cleavage. The gray α carbon representations of YefM with selected residues are shown for reference.
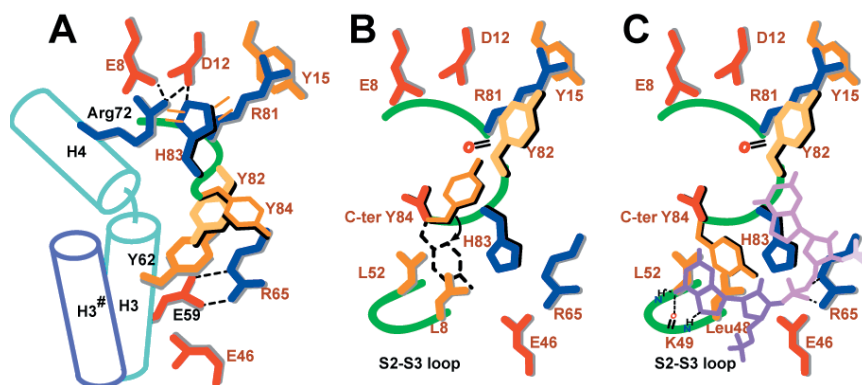

Figure 7

Conformational change at the catalytic site of YoeB. Schematic representations of the active site conformation of YoeB bound to YefM (A), and a transition model from YefM-free form to the active form of YoeB bound to RNA (B and C).

rangement of the RNase catalytic site of YoeB, induced by interaction with YefM (Figs. 6B and 6C). In the YefM-free form, the three catalytic residues of YoeB fold into a canonical coordination seen in microbial RNase Sa. In the complex form, the side chain of the general acid His83 is flipped to the opposite side by binding of YefM. The Arg65 and Glu46 residues are stabilized and occluded by the Glu59 residue of YefM which is perfectly conserved among the YefM antitoxin family. RNA binding by YoeB is probably to change the orientation of the terminal residue Tyr84 in order to stabilize the active site (Fig. 7). The cleavage specificity of YoeB posterior to the purine bases can be explained in terms of hydrogen bond formation between the purine base and the main chain atoms in the S2-S3 loop.

K. Kamada[1] and F. Hanaoka[1,2] ([1]RIKEN, [2]Osaka Univ.)

References
[1] K. Kamada, F. Hanaoka and S. K. Burley, *Mol. Cell*, **11** (2003) 875.
[2] K. Kamada and F. Hanaoka, *Mol. Cell*, **19** (2005) 497.

8-4 Detecting a Bacterial Foe

The innate immune system in multicellular animals has ability to discriminate infectious nonself from non-infectious self. Such fundamental property of innate immune recognition comes from the receptors that have been conceptually named the "pattern-recognition receptors", which recognize unique ligands derived from conserved microbial components such as peptidoglycan, lipopolysaccharide, and flagellin found only in the pathogen but not in the host.

We describe in this work the crystal structure of the ectodomain of peptidoglycan recognition protein LCa (PGRP-LCa), a pattern-recognition receptor that, together with PGRP-LCx, activates innate immune responses in *Drosophila*. PGRP-LCx and –LCa recognize monomeric Gram-negative peptidoglycan via their ectodomains, but the molecular mechanism of ligand recognition was unknown. Previously, four PGRP structures have been reported and they all contain an L-shaped peptidoglycan-docking groove on the surface. PGRP-LCa contains two sequence insertions that are present only in PGRP-LCa but not in PGRP-LCx and any other PGRPs. In this work we determined the crystal structure of the PGRP-LCa ectodomain using synchrotron X-ray beams at the PF BL-5A and showed that the two insertions in the LCa ectodomain disrupt an otherwise continuous surface-docking groove such that the latter cannot accommodate the muropeptide ligand of peptidoglycan (Fig. 8) [1]. We confirmed its deficient binding to monomeric peptidoglycan by biochemical pull-down assays. This work thus provides the molecular basis for the functional difference between PGRP-LCa and PGRP-LCx in recognizing monomeric versus polymeric peptidoglycan. Furthermore, our structural
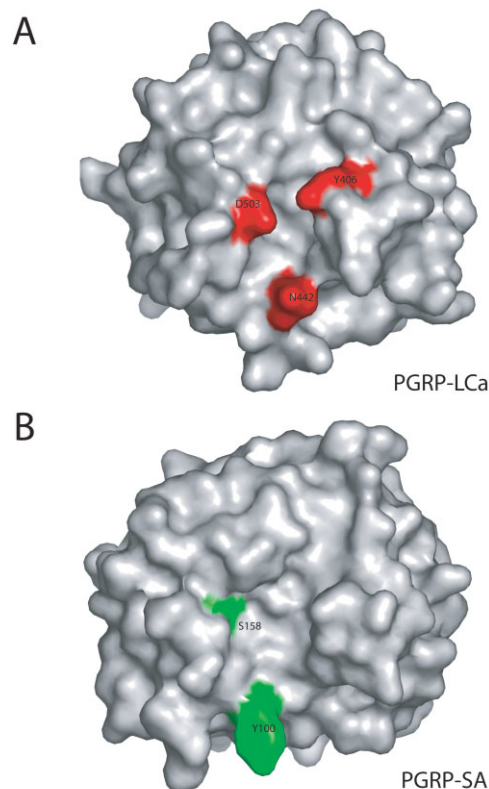

Figure 8
The crystal structure of PGRP-LCa ectodomain (A) contains a disrupted surface groove, where three barricade residues are highlighted. As a result, PGRP-LCa loses its ability to bind muropeptide despite the fact that it has been found to be required for muropeptide recognition. The crystal structure of PGRP-SA, which contains an L-shape peptidoglycan docking groove (B), is shown for comparison.

and biochemical results shed light on the molecular mechanism of muropeptide recognition by the LCa/LCx ectodomains involving *N*-acetyl glucosamine residue and the anhydro bond in the muropeptide ligand, which had been demonstrated to be essential for the immune stimulatory activity. This work has important implication for bacterial recognition by innate immune system.

C.-I. Chang (The Univ. of Texas Southwestern Medical Center)

[1] C.-I. Chang, K. Ihara, Y. Chelliah, D. Mengin-Lecreulx, S. Wakatsuki and J. Deisenhofer, *Proc. Natl. Acad. Sci. USA*, **102** (2005) 10279.

8-5 Crystal Structure of Bispecific Antibody R310 against Modified Protein and DNA with Oxidized Lipids

Reactive oxygen species (ROS) play an important role in cell signaling. However, excess oxidative stress (OS) causes an increased formation of ROSs, resulting in the accumulation of nonenzymatic modifications of human body constituents. Several studies have found oxidative modifications of proteins and the subsequent

accumulation of the modified proteins in cells during aging, OS and in various pathological states, including premature diseases, muscular dystrophy, rheumatoid arthritis, and atherosclerosis [1].

The important agents that bring about the modification of proteins are represented by lipid peroxidation-derived short-chain aldehydes. 4-Hydroxy-2-nonenal (HNE) is a racemic mixture of 4*R*- and 4*S*-enantiomers (Fig. 9a), and is representative of the 4-hydroxy-2-alkenals. HNE is a major product of lipid peroxidation and is believed to be largely responsible for the cyto-pathological effects during OS [2]. Upon reaction with protein, HNE predominantly reacts with the side chain of nucleophilic amino acids such as cysteine, histidine and lysine. This leads to the formation of stable Michael adducts possessing three chiral centers at C-2, C-4 and C-5 in the cyclic hemiacetal (Fig. 9b).

Immunization of animals with *R*-HNE-modified and *S*-HNE-modified carrier proteins led to an establishment of T-cell hybridomas R310 and S412, which are enantioselectively reactive to the HNE-histidine adducts [3]. Interestingly, the primary structure of the anti-*R*-HNE monoclonal antibody (mAb) R310 is homologous to anti-DNA autoantibodies, a hallmark of systemic lupus erythematosus (SLE). The mAb R310 indeed crossreacts with the double-stranded DNA and oligo deoxyguanosine. Moreover, immunoreactivity of mAb R310 is dramatically enhanced by treatment of the DNA with 4-oxo-2-nonenal (ONE), an analog of HNE (Fig .9c). In contrast, mAb S412 shows no significant sequence similarity to the anti-DNA antibodies and no crossreactivity with DNA or modified DNAs [4].

On the basis of these findings, we have evaluated the structural similarity of mAb R310 and anti-DNA mAbs with an X-ray crystallographic analysis. The crystal structure of mAb R310 Fab fragment with HNE-histidine adduct shows that the adduct binds to a hydrophobic pocket in the groove (Fig. 10a), the antigen recognition region, which consists of six complementarity-determining regions (CDRs). It is noted that a pentyl group of the HNE-histidine adduct sticks in the hydrophobic pocket. A common structural feature in the spatial distribution of Tyr and Phe residues (Figs. 10b and 10c) was revealed by comparison of the structure of R310 to that of anti-DNA Fab (DNA-1), which has been shown to bind oligonucleotides by making critical stacking interactions between four tyrosine side chains and the bases. In addition, the basic amino acids are highly conserved in the light chains of anti-*R*-HNE and anti-DNA mAbs. The detailed mechanism of DNA recognition by mAb R310 remains unclear, however, such motifs could be a fundamental aspect of DNA recognition by Abs.
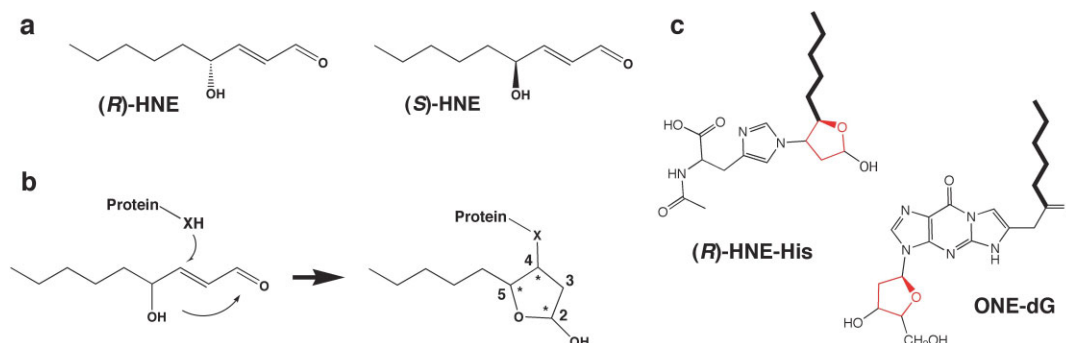

Figure 9
Reaction of (*R*,*S*)-HNE with protein and structure of ONE-2'-deoxyribonucleoside adduct. a) Chemical structures of *R*- and *S*-enantiomers of HNE; b) Formation of the (*R*,*S*)-HNE-protein Michael adducts, which possess three chiral centers (asterisks). X represents the side chain of nucleophilic amino acids, such as cysteine, histidine and lysine. c) Molecular mimicry between HNE-histidine and ONE-2'-deoxyribonucleoside adducts. The pentyl groups (bold lines) and three substituent groups containing furan rings (red lines) are common in both adducts.
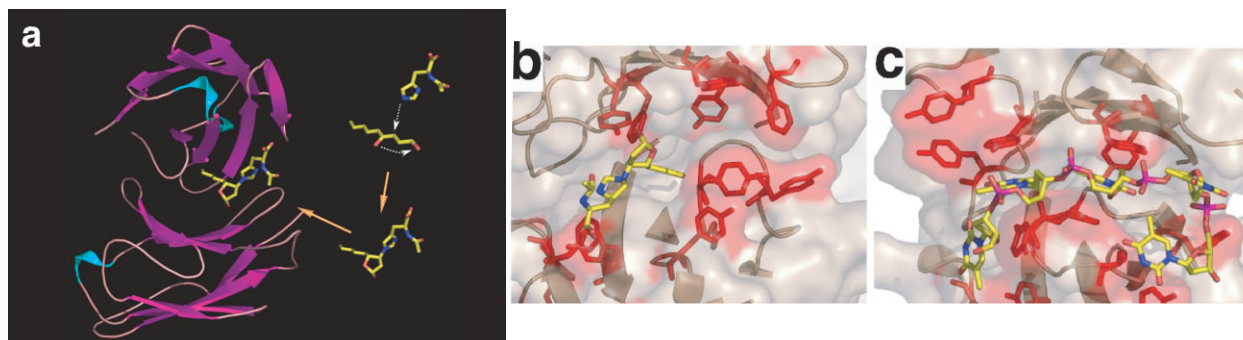

Figure 10
X-ray crystal structure of mAb R310 Fab fragment. (a) Ribbon diagram of mAb R310 Fab complexed with HNE-histidine adduct. Histidine, HNE and HNE-histidine adduct are shown in the wire-frame model. (b) Close-up view of mAb R310 Fab complementarrity determining regions (CDRs). (c) Close-up view of R310 DNA-1 Fab CDRs. The CDRs of (b) and (c) are shown as a ribbon diagram. The tyrosine and phenylalanine residues are shown as a red wire-frame model.

How do the HNE epitopes bring about the production of Abs structurally similar to the anti-DNA autoantibodies? One possibility is that the anti-HNE mAbs may recognize a limited part of the HNE-histidine adducts that form the basis of the DNA and/or modified DNA reactivity. The HNE-histidine adduct is composed of a nitrogen-containing heterocyclic ring, a 2'-deoxyribose-like tetrahydrofuran ring and a pentyl group. These structures could potentially constitute a structural mimic to the DNA and modified DNAs.

Our experiments have shown that the anti-DNA mAb from SLE model mouse crossreacts with the HNE-modified BSA as well as the native DNA. Furthermore, we have confirmed a significant correlation between the serum anti-DNA and anti-HNE titers both in controls and in patients with SLE (unpublished data). These findings offer the attractive hypothesis that the endogenous reactive electrophiles, including HNE, may represent immunologic triggers for human autoimmune disease and allergy.

S. Ito[1], M. Akagawa[2] and K. Uchida[2] ([1]Univ. of Shizuoka, [2]Nagoya Univ.)

References
[1] E. R. Stadtma and R. L. Levine, *Ann. N. Y. Acad. Sci.,* **899** (2000) 191.
[2] H. Esterbauer, R. J. Schaur and H. Zollner, *Free Radic Biol Med,* **11** (1991) 81.
[3] M. Hashimoto, T. Shibata, H. Wsada, S. Toyokuni and K. Uchida, *J. Biol. Chem.*, **278** (2003) 5044.
[4] M. Akagawa, S. Ito, K. Toyoda, Y. Ishii, E. Tatsuda, T. Shibata, S. Yamaguchi, Y. Kawai, K. Ishino Y. Kishi, T. Adachi, T. Tsubata, Y. Takasaki, N. Hattori, T. Matsuda and K. Uchida, *Proc. Natl. Acad. Sci. USA,* **103** (2006) 6160.

8-6 Structural Basis of Alanine Discrimination in Editing Site

Aminoacyl-tRNA synthetases (aaRSs) establish genetic code through the aminoacylation of cognate tRNAs. Because errors in aminoacylation seriously affect the translational fidelity, some aaRSs have developed an additional editing domain that specifically hydrolyzes mischarged tRNAs during evolution. However, though the double sieve discrimination of cognate amino acid via aminoacylation and editing sites has been well-established through studies of class I aaRSs, the discrimination mechanism of evolutionary distinct class II aaRSs is less well understood. Class II alanyl-tRNA synthetase (AlaRS) harbors a cis-editing domain that is specific to mischarged Ser-/Gly-tRNA^{Ala}. As serine/glycine is larger/smaller than alanine, the discrimination of cognate alanine from non-cognate serine and glycine at a single editing site cannot be reasonably explained by canonical size-sieving. On the other hand, interestingly, the autonomous protein AlaX, which shows homology with the AlaRS editing domain, is widely distributed in
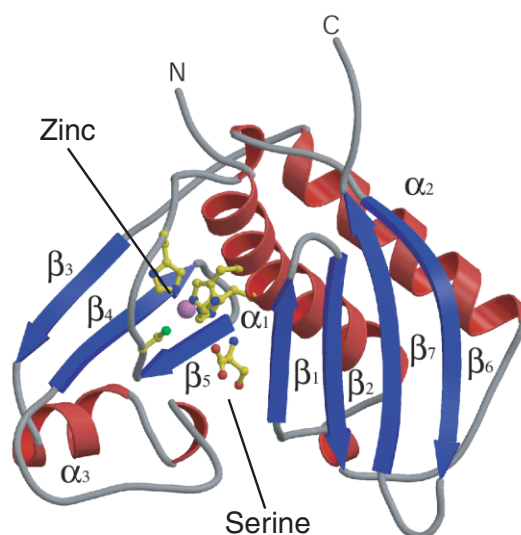

Figure 11
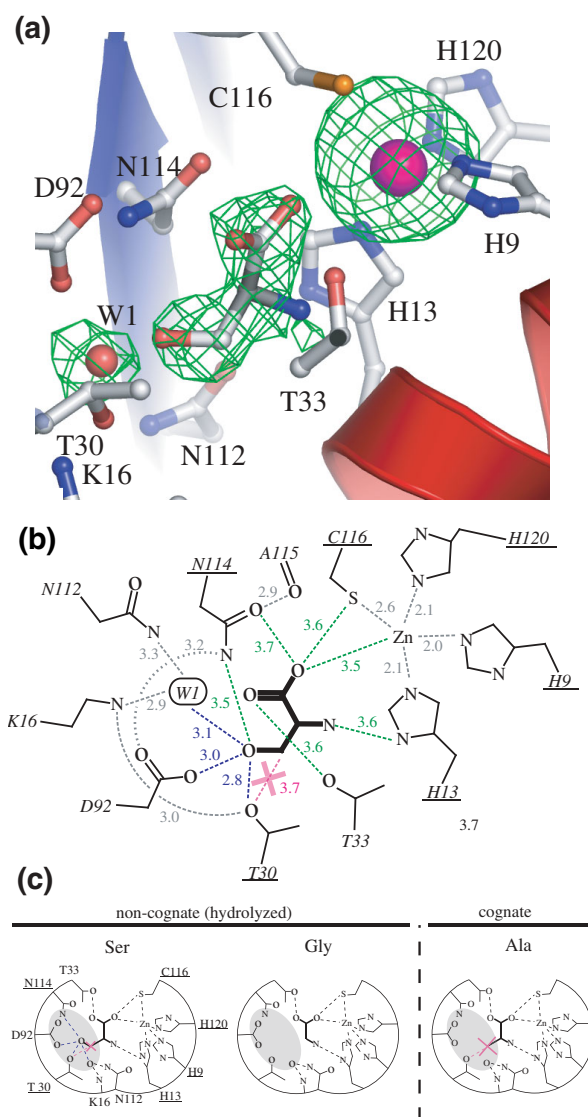Overall structure of the AlaX-serine complex.

Figure 12
(a) Structure of the AlaX editing site. (b) Recognition of serine. Conserved residues are underlined. Distances are indicated (in Å) with dashed lines. The "X" mark indicates the chemical repulsion. (c) The proposed 'chemical discrimination' model at the AlaX editing site.

many organisms and has been shown to have a specific trans-editing activity against mischarged Ser-/Gly-tRNA^{Ala}, although the biological implications remain unclear.

To understand the structural basis of amino acid discrimination in an alanyl system, we have determined the structure of AlaX from archaea in complex with the non-cognate amino acid serine at 2.8-Å resolution, using diffraction data collected at PF-BL-6A [1].
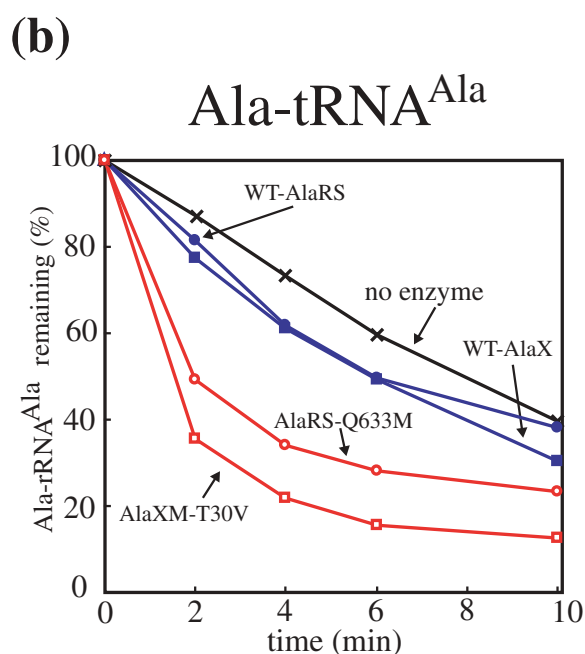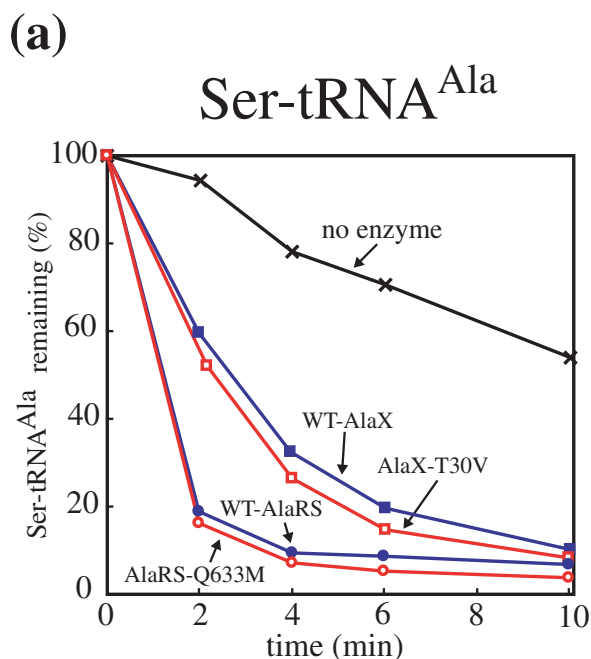
(a)

(b)

The overall structure of AlaX closely resembles the editing domain of threonyl-tRNA synthetase, which shares the zinc-binding motif characteristic of class II aaRS editing domains (Fig. 11). The editing site is located at the center of the molecule, which mainly consists of two parts: the HXXXH and CXXXH zinc-binding motif, and an extremely hydrophilic pocket consisting of Thr30, Asn114, Asp92, and one water molecule (hereafter called W1). The serine molecule is bound deeply within the center of the editing site by orienting its main-chain moiety towards the zinc-binding motif, whereas the side-chain hydroxyl is orientated towards the opposite hydrophilic pocket along with a strong hydrogen bond network with Thr30 hydroxyl, Asp92 carboxyl, and W1 (Fig. 12(a)). Remarkably, Thr30 hydroxyl is located near the β-methylene of the bound serine at the 'entrance' of the pocket, at a distance of 3.7 Å, approximately a Van der Waals' contact (Fig. 12(b)). As Thr30 is highly conserved in prokaryotic AlaX, we envisage that the aliphatic β-carbon of an incoming amino acid will be chemically repulsed by Thr30 hydroxyl. In this situation, a β-methyl from the alanine would not be accommodated with the hydrophilic pocket, whereas a serine hydroxyl would be held strongly by the dense hydrogen bond network with the hydrophilic pocket that compensates for the unfavorable interaction between Thr30 hydroxyl and the β-methylene (Fig. 12(c)). As glycine has no side chain, its discrimination can simply be explained by analogy with canonical size-sieving: it can bind the editing site only by the interaction between the main-chain moiety and the zinc-binding motif.

To confirm this 'chemical discrimination', we replaced the Thr30 hydroxyl by an aliphatic methyl group with a minimum change in size (T30V mutant). As a result, the T30V mutant hydrolyzed cognate Ala-tRNA^{Ala} without changing the activity against non-cognate Ser-tRNA^{Ala} (Fig. 13). This indicates that alanine is discriminated by its chemical nature and not by its size or shape, thus supporting our 'chemical discrimination' model. Furthermore, to confirm whether this model is applicable to the AlaRS cis-editing domain, we mutated the residue in AlaRS corresponding to Thr30 (Gln633), which is also strictly conserved among AlaRS. Again, the Q633M mutant, which resembles the T30V mutant, hydrolyzed Ala-tRNA^{Ala} without any change in the activity against Ser-tRNA^{Ala}. These results together indicate that the 'chemical discrimination' of cognate alanine from non-cognate serine is conserved in both cis- and trans-editing of tRNA^{Ala}.

M. Sokabe, A. Okada, M. Yao, T. Nakashima and I. Tanaka (Hokkaido Univ.)

References
[1] M. Sokabe, A. Okada, M. Yao, T. Nakashima and I. Tanaka, *Proc. Natl. Acad. Sci. USA*, **102** (2005) 11669.

8-7 Novel Ca²⁺ Independent Glycoprotein Cargo Receptors, Emp46p and Emp47p

Figure 14
Crystal structures of the Emp46p (a) and Emp47p (b) CRDs. The secondary structures are highlighted (β-strands belonging to the concave β-sheets, red; β-strands belonging to convex β-sheets, blue; β-strands belonging to β-hairpin, cyan; helices, yellow) and the loops are shown in grey. The bound K⁺ ion in Emp46p is shown as a magenta sphere.

In eukaryotic cells, post-translational modification of secreted proteins and intracellular protein transport between organelles are ubiquitous features. One of the most well-studied systems is the *N*-linked glycosylation pathway in the synthesis of secreted glycoproteins [1]. The *N*-linked glycoproteins are subject to diverse modification and transport from the endoplasmic reticulum (ER) to the *trans*-Golgi network (TGN) in transport vesicles. Incorporation of the cargo glycoproteins into the transport vesicles is mediated by transmembrane cargo receptors, which have been identified as intracellular lectins.

Emp46p and Emp47p, yeast orthologs of ERGIC-53, cycle between the ER and the Golgi apparatus in vesicles coated with coat protein complex II (COPII). They are considered to function as cargo receptors for exporting soluble *N*-linked glycoproteins from the ER [2]. Emp47p is a receptor for Emp46p and is responsible for the selective transport of Emp46p from the ER to the Golgi apparatus by forming hetero-oligomerization between the two proteins [3]. The lumenal domain of Emp46p and Emp47p consists of a carbohydrate recognition domain (CRD) and a putative coiled-coil domain, which are responsible for the formation of the hetero-oligomeric complex.

To investigate the structural basis for the glycoprotein transport by Emp46p and Emp47p, we have determined the crystal structures of the CRDs of Emp46p and Emp47p in the absence and presence of metal ions [4]. The recombinant CRDs of Emp46p and Emp47p were overproduced and purified from *E. coli*. Diffraction-quality crystals were obtained using the hanging-drop vapor-diffusion method, and the diffraction datasets were collected at beamlines BL-5A, BL-6A, BL-18B and AR-NW12A. The structures were solved by the MAD method using SeMet-substituted crystals. Both proteins fold as a β-sandwich (Fig. 14), and resemble ERGIC-53. However, the nature of metal binding is different from that of Ca²⁺-dependent ERGIC-53. Surprisingly, the Emp46p CRD does not bind Ca²⁺ ions but instead a K⁺ ion near the putative carbohydrate binding site (Fig. 15). To the best of our knowledge, structures of lectins in complex with K⁺ ions have never been reported. On the other hand, the Emp47p CRD binds no metal ions at all. The binding of the K⁺ ion to Emp46p appears essential for the transport of a subset of glycoproteins, since the Y131F mutant of Emp46p, which cannot bind the K⁺ ion, fails to rescue the transport in disruptants of EMP46 and EMP47 genes. Furthermore, we showed that the Emp46p CRD binds to glycoproteins carrying high mannose-type glycans but the binding is not affected by the
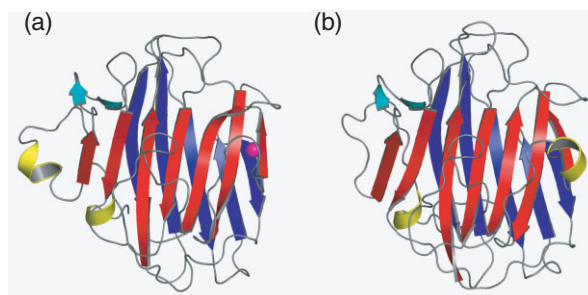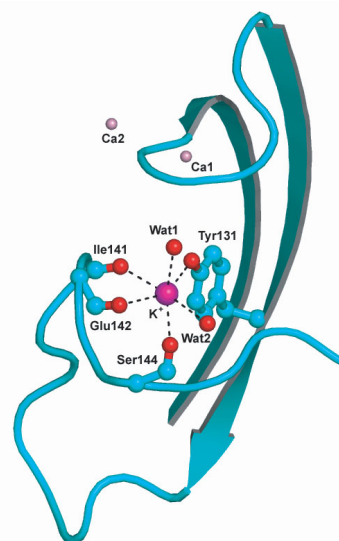

Figure 15
K⁺ binding site of Emp46p. Residues coordinating the K⁺ ion are shown as a ball-and stick model. The position of the K⁺ ion is shown with a magenta sphere. Ca²⁺ sites found in the ERGIC-53 structure are shown as pink spheres (labeled Ca1 and Ca2).

presence of Ca²⁺ or K⁺ ions. These results suggest that Emp46p and Emp47p can be regarded as new Ca²⁺-independent intracellular lectins. Structural determination of the hetero-oligomeric complex of Emp46/47p with high-mannose type glycoproteins and/or glycoconjugates will provide new Ca²⁺-independent carbohydrate recognition modes in trafficking *N*-linked glycoprotein by intracellular lectins.

T. Satoh[1], K. Sato[2], A. Kanoh[3], K. Yamashita[3], Y. Yamada[1], N. Igarashi[1], R. Kato[1], A. Nakano[2,4] and S. Wakatsuki[1] ([1]KEK-PF, [2]RIKEN, [3]Sasaki Inst., [4]The Univ. of Tokyo)

References
[1] A. Helenius and M. Aebi, *Science,* **291** (2001) 2364.
[2] K. Sato and A. Nakano, *Mol. Biol. Cell*, **13** (2002) 2518.
[3] K. Sato and A. Nakano, *Mol. Biol. Cell,* **14** (2003) 3055.
[4] T. Satoh, K. Sato, A. Kanoh, K. Yamashita, Y. Yamada, N. Igarashi, R. Kato, A. Nakano and S. Wakatsuki, *J. Biol. Chem.*, **281** (2006) 10410.

8-8 Crystal Structure of Glucooligosaccharide Oxidase from *Acremonium strictum*, a Novel Flavinylation of 6-S-Cysteinyl, 8α-N1-Histidyl FAD

Glucooligosaccharide oxidase (GOOX) from *Acremonium strictum* was screened for potential applications in diagnostic reagents and industrial biocatalysts. Screening of more than 50 carbohydrates and derivatives showed that D-glucose, maltose, lactose, cellobiose, malto- and cello-oligosaccharides are good substrates, and hence the name of this novel oxidase. To facilitate further characterization and potential industrial use of GOOX, we have cloned and expressed the encoding gene [1]. Interestingly, even though GOOX shares some substrate specificity with glucose oxidase and cellobiose dehydrogenase, it has no sequence similarity to them. In contrast, GOOX displays significant sequence homology to berberine bridge enzyme (BBE)-like proteins. Here we report the crystal structures of the enzyme and of its complex with an inhibitor, 5-amino-5-deoxy-cellobiono-1,5-lactam (ABL) with 1.55-Å and 1.98-Å resolution, respectively [2].

Recombinant protein was expressed using the vector pPICZαA in *Pichia pastoria* KM71, and then isolated by a Toyopearyl Phenyl-650 column. Yellow protein crystals were grown in 25% polyethylene glycol monomethyl ether 550, 10 mM $ZnSO_4$ and 0.1 M MES (pH 6.5), and belong to the $P2_12_12_1$ space group with cell dimensions of a = 53.1 Å, b = 90.9 Å, and c = 111.7 Å. Data collection including platinum anomalous datasets was performed using synchrotron radiation at beamlines BL-5A, BL-6A and AR-NW12A. The protein structure is composed of the FAD-binding domain (residues 1-206, 421-474) and the substrate-binding domain (residues 207-420) (Fig. 16). The F domain consists of two (α + β) subdomains: a small subdomain, comprising a central four β strands (β1-β4), and the second subdomain containing five antiparallel β strands (β5-β9). These two subdomains are surrounded by α-helices, packed against each other, and accommodate the FAD cofactor between them. The S domain possesses a large seven-strand antiparallel β sheet (β10-β16) flanked by five helices and constitutes most of the carbohydrate-binding groove.

Unexpectedly, the FAD cofactor is cross-linked to the enzyme at two attachment sites (Fig. 17). One is the Sγ atom of Cys130 bound to the C6 atom of the iso-alloxazine ring, while the other is the Nδ1 atom of His70 bound to the 8α-methyl group (6-*S*-cysteinyl, 8α-*N*1-histidyl FAD). This is a novel form of covalent flavinylation; it is the first example of 6-*S*-cysteinyl FAD and is the double covalent linkage first identified to date.

ABL resembles cellobionolactone, the oxidation product of cellobiose, with replacement of the endocyclic

O^5 replaced with an NH group. The complex structure provides a structural basis for the substrate specificity and catalytic mechanism: other hexoses and derivatives form either fewer bonds or unfavorable contacts with the amino acid residues surrounding the substrate-binding groove, and GOOX may prefer a β-D-glucosyl residue at the reducing end with the conserved Tyr429 acting as a general base to abstract the OH^1 proton in concert with the H^1 hydride transfer to the flavin N^5. The non-reducing end of the glucose residue can stick out into the solvent. This explains why, because of the open carbohydrate-binding groove, the enzyme is able to utilize oligosaccharides as good substrates (Fig. 18). Four BBE-like proteins including GOOX, a red alga hexose oxidase, a tobacco nectar protein, and a sunflower defence protein, share similar substrate specificity and
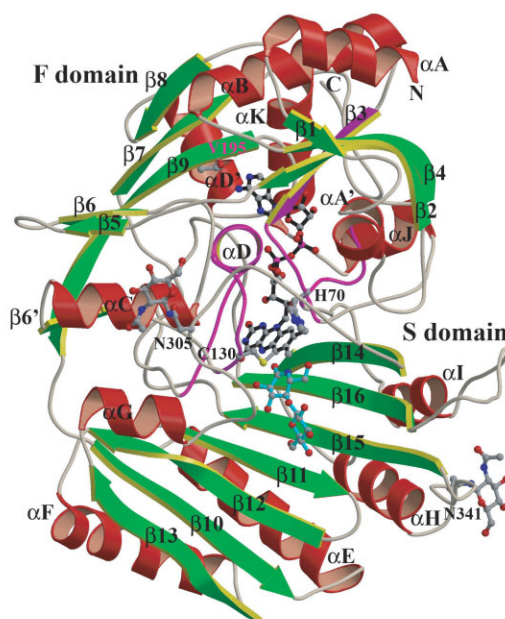

Figure 16

The GOOX structure. The cofactor FAD (*black*), ABL (*cyan*), the linking residues His70 and Cys130, and the glycosylated Asn305 and Asn341 are displayed as *ball-and-stick* representations. The two major FAD-interacting segments are highlighted in *magenta*.
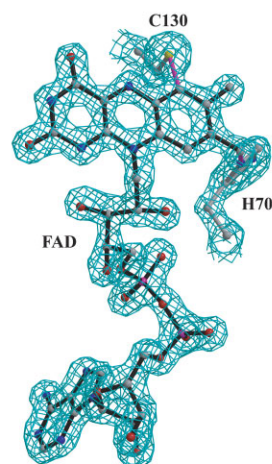

Figure 17

The $2F_o - F_c$ electron density map for the FAD cofactor and the covalently bound His70 and Cys130 contoured at 2σ level, demonstrating the first identified double attachment flavinylation, 6-*S*-cysteinyl, 8α-*N*1-histidyl FAD.

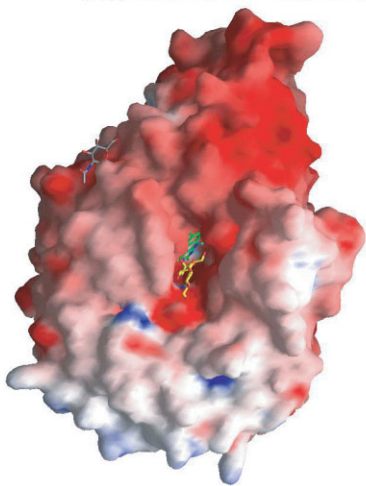F domain, but not a diverse S domain. Therefore, these sugar oxidases have evolved a similar FAD-assisted oxidation mechanism but different substrate recognition, resulting in distinct binding affinities to the mono- and di-sacchardes, with *Km* values ranging from 50 μM to 30 mM.

S. Liaw (National Yang-Ming Univ.)

References
[1] C. Huang, W. Lai, M. Lee, C. Chen, A. Vasella, Y. Tsai and S. Liaw, *J. Biol. Chem.*, **280** (2005) 38831.
[2] M. Lee, W. Lai, S. Lin, C. Hsu, S. Liaw and Y. Tsai, *Appl. Environ. Microbiol.*, **71** (2005) 8881.

8-9 Structure of the Supra- Molecular Pigment in Blue Cornflower

Flower colours ranging from red to blue are mostly produced by anthocyanins [1]. Since the first isolation of an anthocyanin in 1913 as a red oxonium salt from the blue cornflower, *Centaurea cyanus* [2], colour variation has been variously ascribed to either a difference in flower-petal pH or the combination of the pigment with metal ions or other pigments. The blue cornflower pigment (subsequently named protocyanin) has been widely investigated and has been found to contain iron and magnesium ions in combination with anthocyanin and flavone. However, the same anthocyanin has also been discovered in red rose [3], and the mechanism by which the blue colour in cornflower is produced has been unclear for a long time. Recently, we have found that calcium is another essential metal for protocyanin, and successfully reconstructed the pigment using the metals, flavone and anthocyanin [4]. The reconstructed pigment was purified and finally crystallized at a quality suitable for X-ray structure determination. Knowledge of the precise molecular structure of the pigment was expected to be most informative in understanding the mechanism of the blue-colour development. X-ray diffraction measurements were carried out using the dedicated macromolecular-crystallography beamlines BL-6A and AR-NW12A.

The crystal structure of the reconstructed protocyanin was determined at a spatial resolution of 1.05Å. The pigment was found to be a complex molecule consisting of four metal ions (Fe^{3+}, Mg^{2+} and two Ca^{2+} ions), and six anthocyanin [cyanidin 3-*O*-(6-*O*-succinyl-glucoside)-5-*O*-glucoside] and flavone [apigenin 7-*O*-glucuronide-4'-*O*-(6-*O*-malonyl-glucoside)] molecules. The complex molecule has a pseudo three-fold symmetry axis on which the four ions are aligned in the order Ca-Mg-Fe-Ca (Fig. 19a). The four metal ions are coordinated to anthocyanin and flavone; the inner Fe^{3+} is coordinated to three of the anthocyanin molecules and the Mg^{2+} to the other three anthocyanins, and the outer two Ca^{2+} are each coordinated to three flavone molecules (Fig. 19b). Both the anthocyanins and flavones are self-associated in pairs. The Fe^{3+} and Mg^{2+} ions are each coordinated to a different anthocyanin fragment in an anthocyanin pair (Fig. 20a), and the two Ca^{2+} ions are each coordinated to a different flavone fragment in a flavone pair (Fig. 20b). A copigmentation stacking of anthocyanin and flavone was also evident in the protocyanin molecule (Fig. 20c). The C-C and C-O bond lengths in the B-ring of anthocyanin indicate that the anthocyanin is in 4'-keto-quinoidal form.

Figure 19
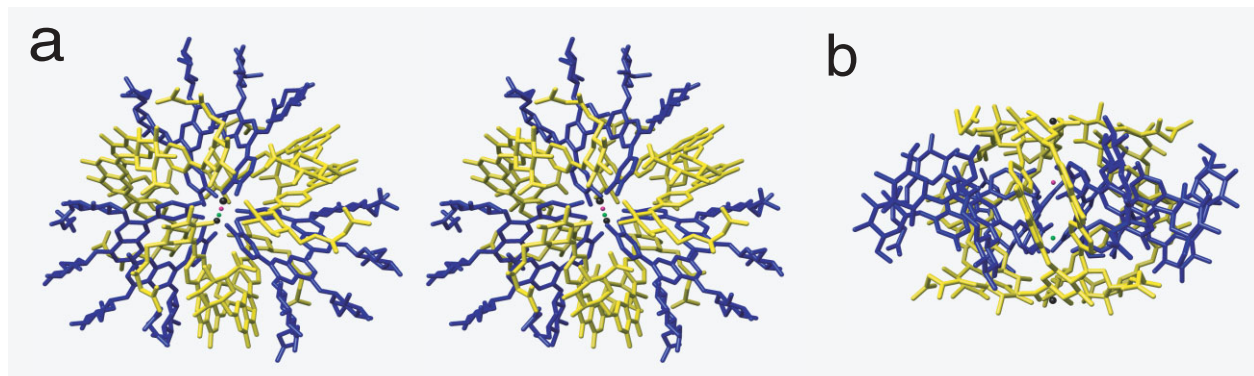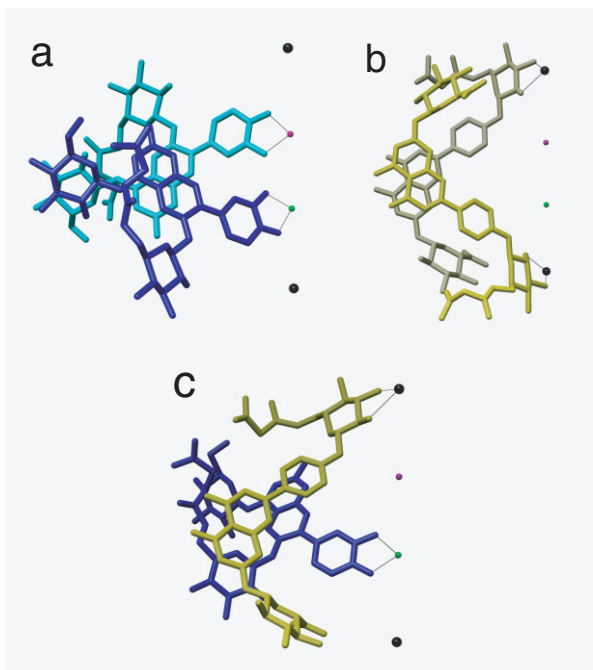Crystal structure of the protocyanin molecule. (a) Stereo view along the pseudo three-fold axis. (b) Side view. Anthocyanin is shown in blue, flavone glycoside in yellow, Fe^{3+} as red balls, Mg^{2+} as green balls, and Ca^{2+} as black balls.

Figure 20
Side views of the stacking of anthocyanin and flavone. (a) One anthocyanin binds to Fe^{3+} (red), while the other to Mg^{2+} (green). (b) Two flavone molecules each bind to one Ca^{2+} (black) in a different site. (c) Copigmentation of anthocyanin and flavone. Anthocyanin binds to Mg^{2+} and flavone to Ca^{2+}

Blue colours are developed mostly by delphinidin-type anthocyanins – for example, commelinin [5]. In protocyanin, however, the blue colour is developed by a cyanidin-type anthocyanin. The chelate formation of Fe^{3+} and Mg^{2+} with the 4'-keto-quinoidal base of anthocyanin apparently plays an important role in blueing in protocyanin. Furthermore, the two Ca^{2+} ions coordinated by flavones may bring about copigmentation as well as the stabilization of the overall protocyanin molecule. The blue colour in protocyanin is therefore developed by a tetra-nuclear metal complex, which may present a new type of supra-molecular pigment [6].

N. Matsugaki[1], M. Shiono[2], K. Takeda[3] ([1]KEK-PF, [2]Kyushu Univ., [3]Tokyo Gakugei Univ.)

References
[1] R. Brouillard and O. Dangles, *The Flavonoids, Advances in Research since 1986* (ed. Harborne, J. B.) 565 (Chapman and Hall, London, 1994).
[2] R. Willstätter and R. W. Everest, J*ustus Liebigs Ann. Chem.*, **401** (1913) 189.
[3] R. Willstätter and H. Mallison, *Justus Liebigs Ann. Chem.*, **408** (1915) 147.
[4] K. Takeda, A. Osakabe, S. Saito, D. Furuyama, A. Tomita, Y. Kojima, M. Yamadera and M. Sakuta, *Phytochemistry* **66** (2005) 1607.
[5] T. Hondo, K. Yoshida, A. Nakagawa, T. Kawai, H. Tamura and T. Goto, *Nature,* **358** (1992) 515.
[6] M. Shiono, N. Matsugaki and K. Takeda, *Nature,* **436** (2005) 791.

8-10 Elucidation of the Structural Change of Inactive Misarranged Recombinant Hyperthermophilic Glutamate Dehydrogenase during Heat Induced Activation under High Temperature

Hyperthermophiles are defined as microorganisms that can grow in high-temperature environments (above 90°C) such as hot springs and submarine volcanoes. It is known that they produce highly thermostable proteins. Proteins are usually produced in large quantities in recombinant cells such as *Escherichia coli*. In some cases, these recombinant proteins form structures different from their native structure. In our study, recombinant glutamate dehydrogenase derived from hyperthermophilic archaea *Pyrobaculum islandicum* (GDH) was produced in its inactive form in *E. coli*. However, upon heating the inactive recombinant GDH (iGDH) to 90°C, the activity increased to a level comparable to that of the native GDH. To better understand the mechanism of this activation, especially regarding structural changes, we carried out small-angle X-ray scattering (SAXS), 1-anilinonaphthalene-8-sulfonic acid (ANS) fluorescence spectroscopy, and differential scanning calorimetry (DSC) studies [1].

The SAXS study revealed that the radius of gyration of the hexameric iGDH was reduced to 47 Å from 55 Å by the application of heat, although the molecular mass of the iGDH was unchanged. The relative hydrophobicity of the GDH was evaluated as a function of the ANS fluorescence intensity. When iGDH was incubated with ANS, the resultant fluorescence spectrum showed an intense emission peak at 446 nm, whereas the emission intensity of the activated GDH (aGDH) was far weaker than that of the iGDH. This indicates a greater number of exposed hydrophobic residues on the surface of the inactive enzyme. The results of the DSC measurements revealed heat-induced activation and denaturation of the enzyme. The middle points of the reactions were 70.2± 0.0°C for activation and 110.3±0.0°C for denaturation, with respective enthalpy changes of 15.5±0.1 and 1880 ±22 kJ/mol - the denaturation enthalpy is more than a hundred times as large as the activation enthalpy.

Although the crystal structure of aGDH has been described previously [2], the structure of the iGDH remains unknown. We generated a low-resolution model structure in an *ab initio* manner (DAMMIN) from the SAXS data and compared it with that of aGDH [3]. The low-resolution structure of aGDH fits well to the observed crystal structure (Fig. 21(a)). Nevertheless, the modeled structure of iGDH has two features that distinguish it from aGDH. The first is its lack of molecular symmetry. The aGDH molecule has 32-point symmetry with one 3-fold axis passing through the two identical trimers
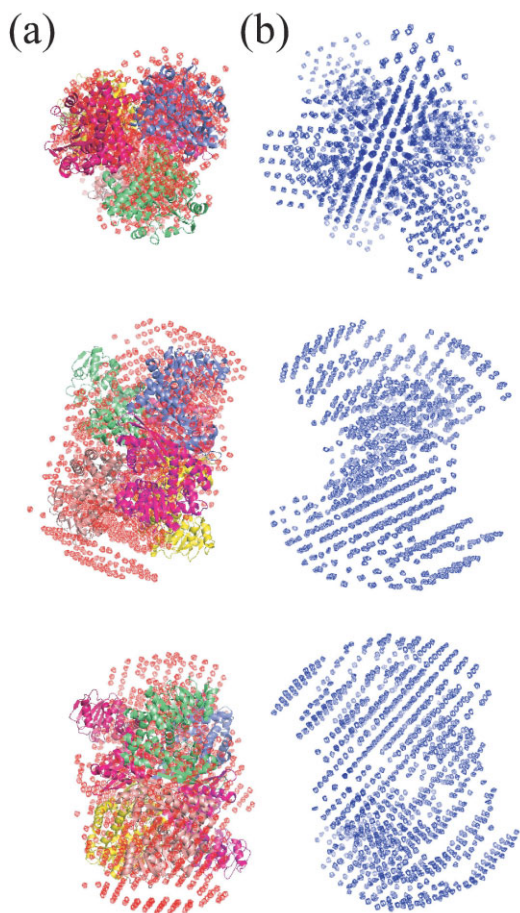
Figure 21
Crystal and low-resolution structures of GDHs. (a) Crystal (ribbon model) and low-resolution (red beads model) structures of aGDH. (b) Low-resolution structure of iGDH (blue beads model). The top row is the hexameric model viewed along the three-fold axis. The middle and bottom rows are the models viewed from different angles of the two-fold axis.

which face each other, yielding a whole molecule with a cylindrical shape (Fig. 21(a), bottom row), and one trimer stacking on the second with a symmetrical interface (Fig. 21(a), top row). In contrast, the structure of iGDH has no symmetry and consequently no subunit from one trimer can superimpose on the corresponding subunit of the other (Fig. 21(b), top row). The second structural feature of iGDH is that it is not cylindrical but is instead more spread out, especially on the surface of the molecule (Fig. 21(b), middle row).

In summary, the inactive enzyme is made up of a loose and unstable subunit arrangement that is perturbed by heat, making the protein settle into a tighter, more stable active arrangement. It can be inferred from the crystal structure of the active enzyme that during this process hydrophobic residues on the surface are synchronously brought to the interior interface between subunits. It thus appears that not only is the oligomerization of GDH necessary for enzymatic activity, but the proper arrangement of the subunits is also essential.

S. Goda[1], M. Kojima[2], H. Sakuraba[1], Y. Hiragi[3] and T. Ohshima[1] ([1]The Univ. of Tokushima, [2]Tokyo Univ. of Pharm. and Life Sci., [3]Kansai Med. Univ.)

References
[1] S. Goda, M. Kojima, Y. Nishikawa, C. Kujo, R. Kawakami, S. Kuramitsu, H. Sakuraba, Y. Hiragi and T. Ohshima, *Biochemistry*, **44** (2005) 15304.
[2] M. W. Bhuiya, H. Sakuraba, T. Ohshima, T. Imagawa, N. Katunuma and H. Tsuge, *J. Mol. Biol.*, **345** (2005) 325.
[3] D. I. Svergun, *Biophys. J.*, **76** (1999) 2879.

8-11 Does Cold Water Act Like Alcohol?

It is of interest that protein denatures at low temperatures [1]. Although this cold denaturation is theoretically predicted, few cases have actually been observed. This is due to the fact that the cold denaturation process generally occurs at temperatures far below the freezing point of water. In most cases, therefore, cold denaturation has been observed either in the presence of a denaturant or under high pressure in order to lower the freezing point and to shift the transition to an accessible temperature range. As a result, depending on the conditions, diverse conformational characteristics have been observed in the cold denatured state.

Recently, we have found that a protein from horse milk, equine β-lactoglobulin (ELG), assumes a novel conformation in the cold denatured state [2]. Small-angle X-ray scattering (SAXS) showed that the radius of gyration of the molecule is close to that in the concentrated denaturant solution (Fig. 22), although more than 30% of the residues were thought to be in α-helical conformation as deduced from a circular dichroism (CD) spectrum [2]. Although helical and expanded conformations are frequently observed in a water-alcohol mixture [3], such conformations are seldom observed in aqueous solution. However the existence of such conformations at low temperatures is reasonable, because the hydrogen-bonded structure should be stable, and the hydrophobic effect which keeps the molecule compact can be expected to be weak at low temperatures.

Two reasons are considered why the helical and expanded conformations are seldom observed in the cold denatured state. Firstly, the denaturants frequently used for the observation of the cold denaturation disrupt the α-helix. In the case of ELG, in fact, the helical CD signal was not prominent in the presence of 4 M urea, although it was significant at 2 M urea [2]. Secondly, the secondary structures of proteins are generally stabilized by non-local interactions among hydrophobic residues. In most cases, therefore, the protein fragments that encompass the α-helix do not assume the α-helix conformation even at low temperatures. In the cold-denatured state, the hydrophobic effect is weakened at low temperature and the α-helix is not stabilized sufficiently by the local interactions alone. ELG has an unusual amino acid sequence, the helical tendency of which is extremely high despite the predominantly
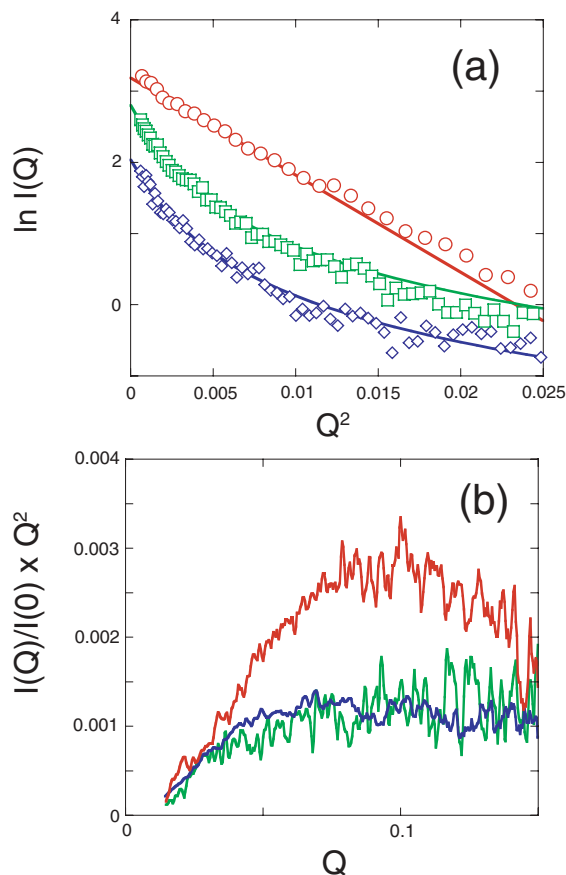
Figure 22
(a) Guinier and (b) Kratky plots of SAXS data for native ELG (red), unfolded ELG in 8M urea (green), and cold-denatured ELG at 2 M urea and –5°C (blue). From the Guinier plots, the radius of gyration is evaluated to be 18 Å for native ELG, 40 Å for unfolded ELG, and 37 Å for cold-denatured ELG. The Kratky plots show that the cold-denatured ELG assumes a conformation close to unfolded ELG. (Reprint from Fig. 5 of Ref. [2], Copyright 2005, with permission from Elsevier.)

β-sheet structure of the protein. The α-helices in the cold-denatured ELG may be stabilized mainly by local interactions.

Even though the observed conformation in the cold-denatured state is similar to that in the alcohol-denatured state, the molecular mechanisms underlying these phenomena may be different from each other. The solubility of hydrophobic substances is increased by the addition of denaturants such as urea and guanidine hydrochloride, by the addition of alcohols, and by lowering the temperature. Protein stability is also decreased by these perturbations through a decline in the hydrophobic effect. However, denaturants and alcohols affect not only the hydrophobic effect but also the hydrogen-bonding properties of peptides and water. Thus, the effects of these additives on protein stability are complex. It is not understood why alcohol promotes helical conformations. In contrast, the temperature effect on hydrogen bonds is predictable from the enthalpy change.

Y. Yamada, K. Fujiwara and M. Ikeguchi (Soka Univ.)

References
[1] P. L. Privalov, *Crit. Rev. Biochem. Mol. Biol.*, **25** (1990) 281.
[2] Y. Yamada, T. Yajima, K. Fujiwara, M. Arai, K. Ito, A. Shimizu, H. Kihara, K. Kuwajima, Y. Amemiya and M. Ikeguchi, *J. Mol. Biol.*, **350** (2005) 338.
[3] Y. O. Kamatari, S. Ohji, T. Konno, Y. Seki, K. Soda, M. Kataoka and K. Akasaka, *Protein Sci.*, **8** (1999) 873.

8-12 Cell-Cycle Arrest in M Phase EGFP-HeLa Cells Caused by Soft X-Ray Micro-Beam Irradiation

The system at BL-27B for irradiating culture cells with micro-beam soft X-rays has excellent characteristics for observing irradiation phenomena occurring in cells *in situ* and for clarifying fundamental problems in radiation biology, such as molecular mechanisms of radiation damage and repair systems in cells, low-dose radiation effects on cells and bystander effects on non-irradiated cells [1]. Using the system cells can be irradiated individually, and a particular cell's nucleus and cytoplasm can be irradiated separately. The system is easy to handle, and appropriate to irradiate living biological systems with simple steps, although the X-ray energy available is limited to 5.35 keV at present.

Recently the problem of why cells in the M phase exhibit higher radiosensitivities than those in the other phases such as G1, S and G2 has attracted much interest in radiation biology, however, the exact mechanism of the different radiosensitivity remains unclear. Mitotic arrest caused by DNA-damaging reagents has been observed and the molecular mechanisms of the arrest have been discussed in detail [2]. However, few studies have been made focusing on the mitotic arrest caused by radiation [3,4].

This study reports on an abnormal cell-cycle progression in the M phase observed using the micro-beam irradiation system at BL-27B, with each single M phase cell in each mitotic stage being irradiated with a 5.35-keV X-ray micro beam focused on the cell nucleus. HeLa cells, genetically modified and expressing EGFP-tagged aurora kinase B, were used in order to recognize the stage of each cell in the M phase [5]. It is generally known that the M phase of cells can be divided into five stages - the prophase, prometaphase, metaphase, anaphase and telophase stages. EGFP-tagged aurora kinase B allowed these five stages to be easily recognized using a fluorescent microscope, as shown in Fig. 23. Each single cell at each stage was irradiated with a monochromatic micro-beam with a size of 10 μm × 10 μm focused on the nucleus. Each irradiated cell was pursued on line to follow the mitotic cell division to the end. The cells were placed in special dishes on line for irradiation at a controlled temperature of 35°C and in a

| Prophase | Prometaphase | Metaphase | Anaphase | Cytokinesis |
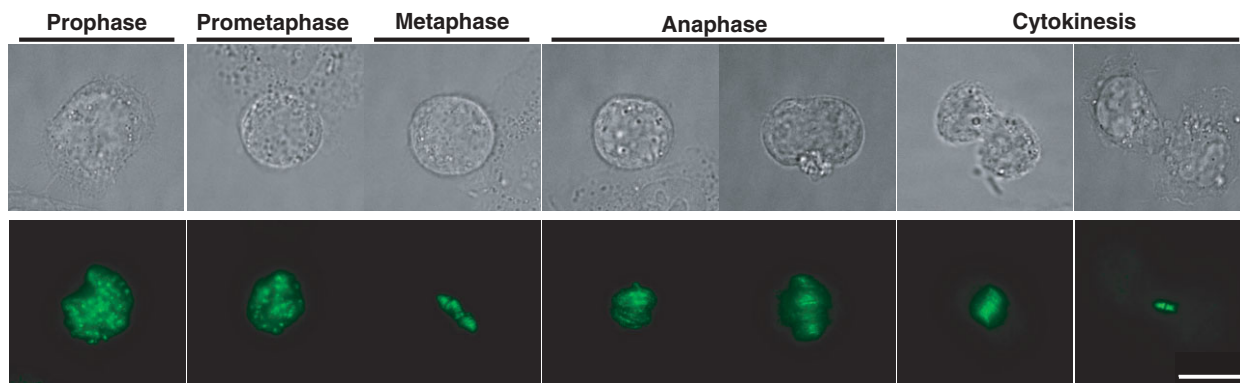
Localization of EGFP- aurora B in M phase

Scale bar: 15 μm
x 60 objective

Figure 23
Images of cell division in HeLa cells obtained using an optical microscope (upper column) and fluorescent microscope (lower column). The stages of the cells in the M phase can be recognized by the localization of the EGFP-Aurora B protein.
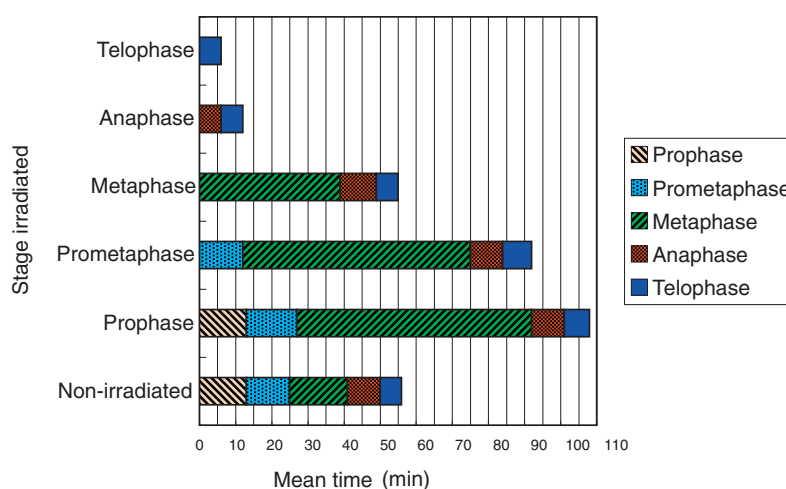

Figure 24
The mean time in each stage of the M phase in non-irradiated or 10 Gy-irradiated cells. The mean time in the M phase for the non-irradiated controls was 56 min and that for the cells irradiated in the prophase was 108 min.

HEPES medium to allow control of the appropriate CO_2 conditions. Thus, non-irradiated cells could maintain normal-cell division in the dish. Each cell at each stage was irradiated with 10 Gy at a dose rate of 20 Gy/min, and the average time in each stage is shown in Fig. 24. These results clearly show that cell-cycle progression in the M phase shows a mitotic arrest due to a delay of the metaphase/anaphase transition. The results also show that cell irradiation in the M phase before the anaphase causes the mitotic arrest, while irradiation following the anaphase does not cause the mitotic arrest in the cells. The dose dependence of the elongation of the M phase was also examined, with the result that a critical radiation dose of 3 - 4 Gy causes the mitotic arrest. In order to clarify the molecular mechanism of the mitotic arrest, checkpoint proteins in the M phase were studied. One of these proteins, MAD2, was observed in the prophase and metaphase using an immunostaining method. Our results also show that the checkpoint mechanism is important in causing the mitotic arrest even if the cells are in the M phase. The structure of DNA damage relating to the mitotic arrest caused by soft X-ray irradiation is now being investigated [6].

K. Takakura[1], Y. Tanno[1], K. Kobayashi[2], M. Tatsuka[3] and E. Gotoh[4] ([1]ICU, [2]KEK-PF, [3]Hiroshima Univ., [4]Nati. Inst. Infectious Diseases)

References
[1] K. Kobayashi, N. Usami, H. Maezawa, T. Hayashi, K. Hieda and K. Takakura, *International Congress Series.* **1258** (2003) 207.
[2] D. V. Bulavin, S. A. Amundson and A. J. Fornace, *Curr. Opin. Genet. Dev.*, **12** (2002) 92.
[3] A. Mikhailov, R. W. Cole and C. L. Rieder, *Curr. Biol.*, **12** (2002) 1797.
[4] A. Royou, H. Macias and W. Sullivan, *Curr. Biol.*, **15** (2005) 334.
[5] M. Murata-Hori, M. Tatsuka and Y. L. Wang, *Mol. Biol. Cell*, **13** (2002) 1099.
[6] E. P. Rogakou, D. R. Pilch, A. H. Orr, V. S. Ivanova and W. M. Bonner, *J. Biol. Chem.,* **273** (1998) 5858.